THE MORPHOLOGICAL CONTENT OF 10 EDisCS CLUSTERS AT $0.5 < z < 0.8$[1,2]

V. DESAI,[3,4] J. J. DALCANTON,[4] A. ARAGÓN-SALAMANCA,[5] P. JABLONKA,[6] B. POGGIANTI,[7]
S. M. GOGARTEN,[4] L. SIMARD,[8] B. MILVANG-JENSEN,[9] G. RUDNICK,[10] D. ZARITSKY,[11]
D. CLOWE,[11] C. HALLIDAY,[12] R. PELLÓ,[13] R. SAGLIA,[14] AND S. WHITE[15]

ABSTRACT

We describe *Hubble Space Telescope* (*HST*) imaging of 10 of the 20 ESO Distant Cluster Survey (EDisCS) fields. Each ~ 40 arcmin^2 field was imaged in the F814W filter with the Advanced Camera for Surveys Wide Field Camera. Based on these data, we present visual morphological classifications for the ~ 920 sources per field that are brighter than $I_{auto} = 23$ mag. We use these classifications to quantify the morphological content of 10 intermediate-redshift ($0.5 < z < 0.8$) galaxy clusters within the *HST* survey region. The EDisCS results, combined with previously published data from seven higher redshift clusters, show no statistically significant evidence for evolution in the mean fractions of elliptical, S0, and late-type (Sp+Irr) galaxies in clusters over the redshift range $0.5 < z < 1.2$. In contrast, existing studies of lower redshift clusters have revealed a factor of ~ 2 increase in the typical S0 fraction between $z = 0.4$ and 0, accompanied by a commensurate decrease in the Sp+Irr fraction and no evolution in the elliptical fraction. The EDisCS clusters demonstrate that cluster morphological fractions plateau beyond $z \approx 0.4$. They also exhibit a mild correlation between morphological content and cluster velocity dispersion, highlighting the importance of careful sample selection in evaluating evolution. We discuss these findings in the context of a recently proposed scenario in which the fractions of passive (E, S0) and star-forming (Sp, Irr) galaxies are determined primarily by the growth history of clusters.

Subject headings: galaxies: clusters: general — galaxies: evolution — galaxies: formation

Online material: machine-readable table

1. INTRODUCTION

Although the morphology-density relation is observationally well established, it is still unclear why the incidence of early type (E+S0) galaxies is higher in overdense regions of the universe. The options are often couched in terms of "nature" versus "nurture." These scenarios describe different paths to qualitatively similar relations between morphology and environment, and are

therefore difficult to disentangle. In the nature scenario, galaxies that end up in high-density environments at low redshift are more likely to have experienced initial conditions leading to an early-type morphology *on formation*. In the nurture scenario, all galaxies, regardless of their local densities at low redshift, have identical probabilities of having formed as early types. The morphology-density relation is then the result of subsequent morphological alterations as galaxies enter increasingly higher density environments as structure grows. Many mechanisms that could produce the required morphological transformations have been suggested, including mergers and galaxy-galaxy interactions (Toomre & Toomre 1972; Icke 1985; Lavery & Henry 1988; Mihos 2004), harassment (Richstone 1976; Moore et al. 1998), gas stripping (Gunn & Gott 1972; Abadi et al. 1999; Quilis et al. 2000), strangulation (Larson et al. 1980; Bekki et al. 2002), and cluster tidal forces (Byrd & Valtonen 1990).

The observed evolution of the morphology-density relation provides an important constraint on models of its origin. Observations of the high-density regions of cluster cores show that while the elliptical fraction has not evolved, the S0 (Sp+Irr) fraction has grown (diminished) by a factor of ~ 2 over the last 5 Gyr (Dressler et al. 1997; Fasano et al. 2000). However, over the same time interval, no evolution is observed at lower densities (Treu et al. 2003; Smith et al. 2005). The morphology-density relation at larger lookback times ($z > 0.5$) has just begun to be explored. Smith et al. (2005) used *Hubble Space Telescope* (*HST*) Wide-Field Planetary Camera 2 (WFPC2) data for six clusters at $0.75 < z < 1.25$ to estimate the early-type fraction as a function of local galaxy surface density. They extended their measurements to low densities (~ 1 Mpc^{-1}) by including field galaxies in *HST* WFPC2 images of the cluster CL0024 at $z = 0.395$. Comparing their results to similar studies at lower redshifts (Dressler 1980b; Dressler et al. 1997; Treu et al. 2003), they found that the early-type fraction has increased steadily since $z \sim 1$ in the densest regions

[3] Division of Physics, Mathematics and Astronomy, California Institute of Technology, Pasadena, CA 91125.

[4] Department of Astronomy, University of Washington, Seattle, WA 98195-1580.

[5] School of Physics and Astronomy, University of Nottingham, Nottingham NG7 2RD, UK.

[6] Université de Genève, Laboratoire d'Astrophysique de l'Ecole Polytechnique Fédérale de Lausanne, Observatoire, CH-1290 Sauverny, Switzerland.

[7] Osservatorio Astronomico di Padova, 35122 Padua, Italy.

[8] Herzberg Institute of Astrophysics, National Research Council of Canada, Victoria, BC V9E 2E7, Canada.

[9] Dark Cosmology Centre, Niels Bohr Institute, University of Copenhagen, DK-2100 Copenhagen, Denmark.

[10] National Optical Astronomy Observatory, Tucson, AZ 85719.

[11] Steward Observatory, University of Arizona, Tucson, AZ 85721.

[12] Osservatorio Astrofisico di Arcetri, 50125 Florence, Italy.

[13] Laboratoire d'Astrophysique de l'Observatoire Midi-Pyrénés, F-31400 Toulouse, France.

[14] Max-Planck-Institut für extraterrestrische Physik, D-85748 Garching bei München, Germany.

[15] Max-Planck-Institut für Astrophysik, D-85748 Garching bei München, Germany.

($\sim$1000 Mpc^{-2}), has increased only since $z \sim 0.5$ in moderate-density regions ($\sim$100 Mpc^{-2}), and has remained constant since $z \sim 1$ in the lowest density regions ($<$10 Mpc^{-2}). Postman et al. (2005) find compatible results in their study of the morphology-density relation using *HST* Advanced Camera for Surveys (ACS) imaging of seven $z \sim 1$ clusters. Smith et al. (2005) suggest a nurture scenario to explain the observed evolution in the morphology-density relation. If structure growth is hierarchical, the densest regions at any redshift collapsed the earliest. Thus, if environmental processes can modify a universal initial mix of morphologies through a transformation from late to early types, these processes would have had a longer time to operate in increasingly dense regions. In addition, the efficiency of such transformations could be density-dependent.

To discover whether environmental processes, rather than initial conditions, drive the differential evolution of the morphology-density relation, we must first demonstrate that nature scenarios cannot reproduce the observations. If we find that environmental factors are indeed important, it is critical to identify the responsible mechanisms. The current data are insufficient to discriminate among the alternative models. For this, we require a full mapping between galaxy properties and environment. Toward this goal, we present the morphological fractions in 10 rich clusters at $0.5 < z < 0.8$, drawn from the ESO Distant Cluster Survey (EDisCS; White et al. 2005).[16] Because strong evolution has been observed in high-density regions, clusters are a critical environment to probe. The redshift range of our study bridges a gap between those of Dressler (1980a), Fasano et al. (2000), and Dressler et al. (1997) at low redshift and those of Smith et al. (2005) and Postman et al. (2005) at high redshift. The EDisCS clusters represent a significant increase in the number of well-studied clusters at high redshift. Because the mean age of clusters decreases with increasing redshift, the scatter in cluster properties may also increase with redshift. Thus, large samples are necessary to disentangle evolution from cluster-to-cluster variations. Finally, we measure morphologies from high-quality *HST* ACS images, allowing us to distinguish S0's from other early types. As described above, the S0 population appears to have increased at the expense of the Sp+Irr population since $z = 0.5$. Thus, tracing the S0 population to high redshifts may place important constraints on their formation.

This paper is organized as follows. In § 2 we describe the EDisCS sample. In § 3 we describe the *HST* ACS data used to measure morphologies. Our classification procedure and Hubble types for all galaxies with $I_{auto} < 23$ mag are presented in § 4. In § 5 we describe our method of quantifying the morphological content in each cluster. Our results are presented in § 6, and our conclusions regarding them can be found in § 7.

Results are presented for two sets of cosmological parameters to allow a direct comparison with previous work ($\Omega_0 = 1$, $\Lambda = 0$, $H_0 = 50$ km s^{-1} Mpc^{-1}) and to provide the corresponding estimate for the currently standard cosmology ($\Omega_0 = 0.3$, $\Lambda = 0.7$, $H_0 = 70$ km s^{-1} Mpc^{-1}). In the remainder of this paper we refer to these as the classic cosmology and the *WMAP* cosmology, respectively.

2. THE ESO DISTANT CLUSTER SURVEY (EDisCS)

The 10 clusters included in this study are a subset of the ESO Distant Cluster Survey, an extensive program to obtain spectroscopy and multiwavelength photometry for 20 galaxy clusters at $0.4 < z < 1$. Details of the goals and data sets associated with

[16] See http://www.mpa-garching.mpg.de/galform/ediscs/index.shtml.

this survey are documented by White et al. (2005), but we briefly summarize below.

The clusters chosen to be part of EDisCS were drawn from the Las Campanas Distant Cluster Survey (LCDCS) catalog, which consists of optically selected clusters identified from fluctuations in the extragalactic background light (Dalcanton 1996; Zaritsky et al. 1997; Gonzalez et al. 2001). The redshifts of the LCDCS cluster candidates were initially estimated from the apparent magnitude of the brightest cluster galaxy (BCG). The candidates were divided into an intermediate-redshift group ($z \sim 0.5$) and a high-redshift group ($z \sim 0.8$). Shallow two-color imaging was obtained at the Very Large Telescope (VLT) for the 30 brightest candidates in each group. A sample of 20 EDisCS clusters was selected based on the presence of a red sequence and a BCG of the appropriate magnitude (Gonzalez et al. 2001). These 20 clusters were then imaged more deeply at the VLT in *BVI* (45 minutes) for the $z \sim 0.5$ candidates and in *VRI* (2 hr) for the $z \sim 0.8$ candidates. These data, covering a $6.5' \times 6.5'$ region in the field of each cluster, are presented in White et al. (2005) and form the basis of the weak-shear analysis presented by Clowe et al. (2006). Additional near-infrared imaging was obtained with SOFI at the New Technology Telescope (NTT) in K_s for the $z \sim 0.5$ candidates and in JK_s for the $z \sim 0.8$ candidates (A. Aragón-Salamanca et al. 2007, in preparation). The near-infrared imaging covers approximately $6' \times 4.2'$ in the fields of the intermediate-redshift clusters and $5.4' \times 4.2'$ in the fields of the high-redshift clusters. The optical and near-infrared imaging were used to measure photometric redshifts, as described in R. Pelló et al. (2007, in preparation).

An initial phase of spectroscopy consisted of relatively short exposures of a single slit mask per cluster. One cluster with an estimated redshift of $z \sim 0.8$ was revealed as a superposition of weak groups and was rejected from the sample. These spectra revealed that the remaining 19 clusters have redshifts in the range $0.4 \lesssim z \lesssim 1$. Deeper spectroscopic exposures ($\sim$2 hr each for galaxies with $18.6 \le I(r = 1'') \le 22$ mag in intermediate-redshift clusters; $\sim$4 hr each for galaxies with $19.5 \le I(r = 1'') \le 23$ mag in high-redshift clusters) of 3–5 masks per field were then taken and are of sufficient quality to provide information about the stellar populations and internal dynamics of the target galaxies. The spectroscopic observations are described in Halliday et al. (2004) and B. Milvang-Jensen et al. (2007, in preparation).

The ground-based EDisCS imaging and spectroscopy go a long way toward characterizing both the clusters themselves and the galaxies within them. At the high redshifts of the EDisCS sample, however, only *HST* can provide the spatial resolution necessary to provide robust morphologies. Motivated by the issues discussed in § 1, we obtained *HST* imaging for the 10 highest redshift EDisCS clusters, listed in Table 1 along with their basic physical parameters. Cluster 9 (cl1232-1250) was drawn from the EDisCS intermediate-redshift sample, and the remainder were drawn from the high-redshift sample.

3. *HST* ACS DATA

The *HST* observations were designed to coincide as closely as possible with the coverage of the ground-based optical imaging and spectroscopy, within guide-star constraints. The ground-based optical data cover a $6.5' \times 6.5'$ region around each cluster, with the cluster center displaced by $1'$ from the center of the region. For reference, the ACS Wide Field Camera has a field of view of roughly $3.5' \times 3.5'$. Balancing scientific motives for going deep over the entire field against a limited number of available orbits, we tiled each $6.5' \times 6.5'$ field in four pointings, with one additional deep pointing on the cluster center (taken as the location of the

TABLE 1
THE EDisCS *HST* SAMPLE

Number	Name	R.A. (J2000.0)	Decl. (J2000.0)	z	σ (km s^{-1})	$R_{200,1}$ (Mpc)	$R_{200,2}$ (Mpc)
1..........................	cl1037-1243	10 37 51.4	−12 43 26.6	0.58	319^{+53}_{-52}	0.56	0.57
2..........................	cl1040-1155	10 40 40.3	−11 56 04.2	0.70	418^{+55}_{-46}	0.65	0.70
3..........................	cl1054-1146	10 54 24.4	−11 46 19.4	0.70	589^{+78}_{-70}	0.92	0.99
4..........................	cl1054-1245	10 54 43.5	−12 45 51.9	0.75	504^{+113}_{-65}	0.75	0.82
5..........................	cl1103-1245b	11 03 36.5	−12 44 22.3	0.70	252^{+65}_{-85}	0.39	0.42
6..........................	cl1138-1133	11 38 10.2	−11 33 37.9	0.48	732^{+72}_{-76}	1.41	1.40
7..........................	cl1216-1201	12 16 45.3	−12 01 17.6	0.79	1018^{+73}_{-77}	1.47	1.61
8..........................	cl1227-1138	12 27 58.9	−11 35 13.5	0.64	574^{+72}_{-75}	0.95	1.00
9..........................	cl1232-1250	12 32 30.3	−12 50 36.4	0.54	1080^{+119}_{-89}	1.95	1.99
10.........................	cl1354-1230	13 54 09.8	−12 31 01.5	0.76	648^{+105}_{-110}	0.96	1.05

NOTE.—Units of right ascension are hours, minutes, and seconds, and units of declination are degrees, arcminutes, and arcseconds. The coordinates are the positions of the brightest cluster galaxy. The redshifts (z) and line-of-sight cluster velocity dispersions (σ) were taken from Halliday et al. (2004) and B. Milvang-Jensen et al. (2007, in preparation). The values of the virial radius, R_{200}, listed in cols. (6) and (7) were computed with eq. (1) in Poggianti et al. (2006) using the classic cosmology and the *WMAP* cosmology, respectively, as described in § 1.

BCG). The resulting exposure time per pixel is 2040 s, except for the central $3.5' \times 3.5'$, which has an exposure time per pixel of 10,200 s. The deep central pointing probes to lower surface brightness, fainter magnitudes, and larger galactic radii in the region of the cluster containing the most galaxies. The centers of the structures ultimately chosen for spectroscopic follow-up in the cl1103-1245b and cl1227-1138 fields are somewhat offset from those anticipated at the time the *HST* observations were taken. All exposures were taken under LOW SKY conditions to maximize our surface brightness sensitivity.

The ACS calibration pipeline, CALACS version 4.3 (2003 June 6) debiased, dark-subtracted, and flat-fielded our ACS images "on the fly" when they were requested from the *HST* archives. Known bad pixels and saturated data were also flagged in accompanying data quality (DQ) arrays. Approximate world coordinate system (WCS) headers were provided. The resulting images were returned by the archive with the FLT suffix. In addition, images that were cosmic-ray split were combined and returned with a CRJ suffix.

To produce a mosaic, we required precise offsets between the 32 FLT images retrieved for each cluster. The approximate WCS headers provided were insufficient for this purpose. We found that the offsets between cosmic-ray split images were negligible. We therefore computed the necessary shifts between pointings using the higher signal-to-noise CRJ images. The shifts could not be computed using the retrieved CRJ files because they had not been undistorted. We therefore drizzled each CRJ image separately, using the approximate WCS headers provided. Because each undistorted CRJ image overlaps the central pointing, one of the images centered on the cluster center was chosen as the reference image. Shifts between the reference image and each undistorted CRJ image were then computed using cross-correlation.

Combination of the FLT images using the resulting shifts was accomplished using MultiDrizzle, a Python code written by Anton Koekemoer to run under PyRAF, the Python-based interface to the Image Reduction and Analysis Facility (IRAF). MultiDrizzle automatically removes cosmic rays and combines dithered images using PyDrizzle, which has been developed by the Science Software Branch at the Space Telescope Science Institute. For each of the 32 FLT images per cluster, MultiDrizzle included negative bad pixels in the data quality array, subtracted the sky, and separately drizzled and undistorted each image. Next it created a median

image from these separately drizzled images using shifts computed from the headers along with the user-supplied refinement shifts described above. This median image, relatively free of cosmic rays, was compared to the input images to identify cosmic rays. The median image was then redistorted to create cosmic-ray masks. These masks were used in the final image combination step using drizzle and the lanczos3 kernel, which provided optimal noise properties.

4. GALAXY MORPHOLOGIES

We visually classified all galaxies brighter than $I_{auto} = 23$ mag. Here I_{auto} is the SExtractor (Bertin & Arnouts 1996) AUTO magnitude measured on the *I*-band VLT images and is an estimate of the total magnitude of a galaxy in the Vega system. This magnitude does not include an aperture correction, nor has it been corrected for Galactic extinction. The limit was set both to ensure robust classifications and to provide a tractable sample of $\sim$9200 galaxies.

Our classifications are most useful if they conform to systems adopted by previous studies. For this reason, each classifier trained on the *HST* WFPC2 images and visual morphological catalogs of the $0.3 < z < 0.5$ MORPHS clusters, using the same procedure described in Smail et al. (1997). For uniformity, each classifier used the same IRAF script to examine and classify EDisCS galaxies. This script displays two side-by-side versions of a 200 × 200 square pixel cutout centered on each galaxy meeting the magnitude limit described above. One version is on a log scale between −0.1–2 DN s^{-1}, while the other is on a log scale between −0.1–25 DN s^{-1}. Together, these displays allowed classifiers to inspect the galaxies from their high surface brightness cores to their low surface brightness outer features. In general, we found that the depth and quality of the EDisCS ACS data were similar to or better than the MORPHS WFPC2 data for lower redshift clusters.

Classifications were performed by five of the authors (A. A. S., J. J. D., V. D. , P. J. , and B. P.). Each classified the galaxies in three to six clusters. For a given galaxy, the final Hubble type was based on the classifications of two or more of the authors. First, the Revised Hubble Type was translated into a T-type according to the scheme presented in Table 2. Classifications appended by one question mark were given half weight; those appended by two question marks were given one-quarter weight. If a classifier specified two types separated by a slash, the first

TABLE 2
Notes on Parameters in Morphological Catalogs

Heading	Description
ID	EDisCS ID
RA	Right ascension in decimal degrees (J2000.0)
DEC...........................	Declination in decimal degrees (J2000.0)
I_{auto}	Total I magnitude; SExtractor MAG_AUTO parameter measured from ground-based I-band images
Type...........................	Star=-7, nonstellar but too compact to see structure=-6, E=-5,
	S0=-2, Sa=1, Sb=3, Sc=5, Sd=7, Sm=9, Irr=11,
	no HST data corresponding to ground-based object=111, unclassifiable=66
S0 disk flag	If any of the classifiers noted that the B/D ratio is small but the disk is featureless, this flag is 1.
Bar flag	If any of the classifiers noted the presence of a bar, this flag is 1.
Edge-on flag..............	If any of the classifiers noted that this galaxy is edge-on, this flag is 1.
Small flag...................	If any of the classifiers noted that this galaxy is small, this flag is 1.
LSB flag.....................	If any of the classifiers noted that this galaxy is low-surface-brightness, this flag is 1.
Defect flag..................	If any of the classifiers noted that the image of this galaxy was defective,
	due for example to cosmic rays or incomplete coverage, this flag is 1.
Dust flag.....................	If any of the classifiers noted the presence of dust in the galaxy, this flag is 1.
Disturbance flag	If any of the classifiers noted that this galaxy is disturbed, this flag is 1.
Comments	Additional comments by any of the classifiers

Note.—The morphological catalogs are published in the electronic edition of the *Astrophysical Journal*.

was given three-quarters weight and the second was given one-quarter weight. All T types submitted for a given galaxy were then ranked by their frequency. The final Hubble type was then chosen from the highest ranked T types. In general, the highest ranked T type was chosen. If there were two equally ranked classifications, one was chosen randomly. If there were three or more equally ranked classifications, the differences in T types were computed between them. If there were no gaps smaller than three T types, the median value was chosen. If there was one gap smaller than three T types, one of the two similar classifications was chosen at random. If there was more than one gap smaller than three T types, the median value of all classifications was chosen.

The main results of this work are sensitive to how accurately galaxies can be placed into the broad categories of elliptical (E), S0, and late (Sp+Irr). Although accuracy in this case is difficult to quantify, we can test how consistently galaxies are placed in the same bin by different classifiers. Using ∼900 galaxies down to $I_{\mathrm{auto}} = 23$ mag in cl1216-1201, all of which were assigned a Hubble type by all classifiers, we computed the raw fractions for each classifier, uncorrected for the presence of foreground and background galaxies. The root mean variance for any morphological fraction is ≲0.10, which is comparable to the error computed from Poisson statistics.

There is some controversy surrounding the ability of morphologists to distinguish between E and S0 galaxies, especially at high redshifts. For this reason, some previous investigators chose to lump E and S0 galaxies together into an early-type class. For easy comparison with these works, in the following we have plotted and tabulated our results for early types as well as for E and S0 galaxies separately. However, because the S0 population is strongly evolving in clusters at $z < 0.5$, it is important to track this population at higher redshifts. Comparing the EDisCS ACS data to the MORPHS WFPC2 data gives the impression that we can distinguish S0's from ellipticals with the same accuracy for the EDisCS sample as was obtained with the MORPHS sample. To test this impression, we have performed a quantitative analysis of the light distributions of E and S0 galaxies within cl1216-1201, which is our highest redshift cluster and which has been visually examined by all classifiers. Specifically, we used the ELLIPSE task

in the Space Telescope Science Data Analysis System (STSDAS) package of IRAF to measure the surface brightness of a series of isophotal ellipses in each galaxy as a function of semimajor axis. For each step, the semimajor axis is increased by a factor of 1.1. The ELLIPSE task was allowed to vary the ellipticity and position angle of the ellipses within a given galaxy. For each surface brightness profile, we fit a bulge+disk model of the form

$$I_{\mathrm{bulge}}(r) = I_e \exp\left(-7.67[(r/r_e)^{1/4} - 1]\right) \tag{1}$$

and

$$I_{\mathrm{disk}}(r) = I_0 \exp\left(-r/r_d\right), \tag{2}$$

where the total surface brightness is given by $I_{\mathrm{bulge}} + I_{\mathrm{disk}}$. We considered three parameters for which E and S0 galaxies should display different distributions: (1) the width of the ellipticity distribution in a given galaxy, R, defined as the interquartile range of all values of the ellipticity for a given galaxy; (2) the bulge-to-total fraction B/T; and (3) χ^2 goodness-of-fit from fitting the $r^{1/4}$ law (i.e., only bulge, no disk). The differential and fractional cumulative distribution functions for these three parameters are plotted in Figure 1. At a statistically significant level, S0's display larger ellipticity distribution widths than ellipticals. The presence of a disk in a galaxy will result in a wider range of ellipticities, since the ellipticity of the galaxy changes as the disk begins to dominate the surface brightness profile. Likewise, the B/T fractions for visually classified ellipticals appear to be skewed to higher values compared to S0's, as expected. This is confirmed by a two-sided Kolmogorov-Smirnov test. Finally, a higher fraction of ellipticals have small values of χ^2, indicating a better fit to a pure bulge model. However, the differences in the χ^2 distribution are not significant. The overall results of these tests are that visually classified S0's have quantitatively different surface brightness profiles than visually classified ellipticals. Although in some individual cases it is difficult for visual classifiers to differentiate between E's and S0's, it is clear that, in a statistical sense, objects visually classified as E's and S0's form two distinct populations with objectively measurable physical differences. More sophisticated
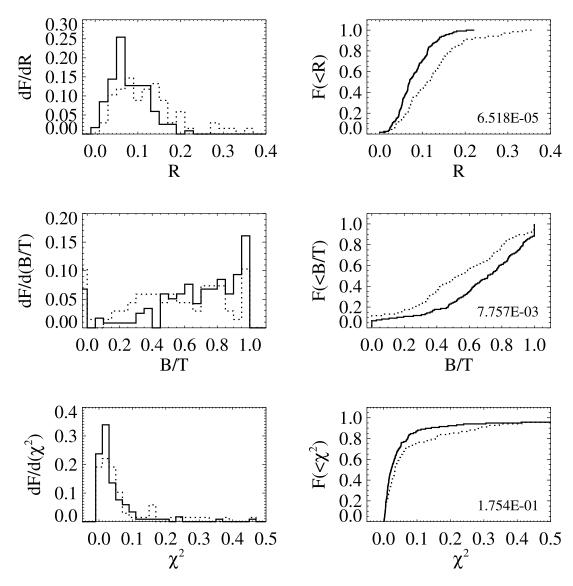
FIG. 1.—Comparison of parameters derived from one-dimensional profile fits to visually classified ellipticals and S0's down to $I_{auto} = 23$ mag in cl1216-1201. From top to bottom, this figure shows the fractional differential (*left*) and cumulative (*right*) distribution functions of the width of the ellipticity distribution within a given galaxy (R), the bulge-to-total fraction (B/T), and the χ^2 goodness-of-fit parameter for a pure de Vaucouleurs component (see § 4). The solid lines indicate the distributions for ellipticals, and the dotted lines indicate the distributions for S0 galaxies. The significance levels of the two-sided Kolmogorov-Smirnov tests comparing the E and S0 distributions are shown in the bottom right of the cumulative distribution plots. The R and B/T distributions for E's and S0's are different at very high significance levels, while the χ^2 goodness-of-fit parameters are different at a low significance level. These results show that galaxies that are classified as E's are structurally distinct from those classified as S0's.

two-dimensional profile fits will be presented in L. Simard et al. (2007, in preparation).

5. ANALYSIS

The goal of this paper is to quantify the morphological content of the EDisCS clusters. In particular, we discuss the overall fractions of E, S0, and late-type galaxies in our clusters and compare them to the fractions found in clusters spanning a range of redshifts. Following Dressler et al. (1997) we do not include galaxies that were unclassifiable (types −6 and 66 in Table 2) in our analysis. To facilitate a fair comparison with other samples, we compute the morphological fractions as consistently as possible with previous work. In the following subsections, we describe the key elements of our analysis.

5.1. *Magnitude Range*

Early types preferentially occupy the bright end of the galaxy luminosity function, while late types dominate the faint end (e.g.,

Blanton et al. 2001; Goto et al. 2002; Zucca et al. 2006). Thus, morphological fractions depend on the range of absolute magnitudes sampled. Morphological fractions in the MORPHS clusters were determined using apparent magnitude cuts in I_{814} designed to correspond to a V-band absolute magnitude of $M_V = -20$ mag (Dressler et al. 1997), but in actuality corresponding to $M_V = -19$ mag due to a transcription error (Fasano et al. 2000). However, Fasano et al. (2000) reanalyzed the MORPHS data with the intended limiting absolute magnitude and additionally analyzed nine clusters with $0.1 < z < 0.25$ in the same manner, providing an ideal comparison sample for the EDisCS clusters. We therefore adopt an absolute magnitude limit of $M_V = -20$ mag. For a given cluster, the limiting apparent magnitude in the I-band is then given by

$$I_{auto,lim} = M_V + 5 \log_{10}(d_{L,pc}) - 5 - (M_V - M_I) + k_I, \quad (3)$$

where $d_{L,pc}$ is the luminosity distance of the cluster in parsecs (calculated in either the classic or *WMAP* cosmology, as indicated),

$M_V - M_I$ is the rest-frame color, and k_I is the I-band k-correction. We adopt the rest-frame color and Cousins I-band k-corrections for an elliptical galaxy, as presented in Poggianti (1997). Equation (3) results in values of $I_{\mathrm{auto,lim}}$ ranging from 21.3 to 23.3 mag, the faintest values being slightly fainter than the limit of our visual classifications. Given the errors in the k-corrections relative to these differences, we adopt $I_{\mathrm{auto,lim}} = 23$ mag in these instances. This occurs for cl1216-1201 when using the *WMAP* cosmology and for cl1054-1245, cl1216-1201, and cl1354-1230 when using the classic cosmology.

5.2. Aperture

Clusters exhibit a radial gradient in their morphological fractions; the centers of clusters contain a larger fraction of ellipticals than the outskirts (e.g., Melnick & Sargent 1977; Goto et al. 2004; Thomas & Katgert 2006). Thus, in comparing the overall morphological fractions across clusters, one must choose a consistent aperture. The MORPHS project has set the standard for the aperture within which to compute morphological fractions. Most studies of the morphological fractions of galaxy clusters at other redshifts have used a similarly sized aperture. So that we may assess the level of evolution between the morphological studies presented in the literature and those conducted with EDisCS data, we adhere to this precedent and adopt a circular aperture of radius 600 kpc (classic cosmology).

Since the radial density profiles of clusters vary, the average galaxy density within a fixed metric aperture will also vary. We therefore also calculated the morphological fractions within an aperture that scales with R_{200}, the radius within which the average mass density is equal to 200 times the critical density. The derived R_{200}-values were computed using equation (8) in Finn et al. (2005) and are listed in Table 1 for both the classic and *WMAP* cosmologies. Unfortunately, our imaging data is complete out to R_{200} for only cl1040-1155, cl1054-1146, cl1054-1245, and cl1354-1230. We therefore use a radius of $0.6\,R_{200}$, which keeps the analysis area within the imaging region for all clusters except for cl1227-1138 and cl1232-1250. The fraction of the analysis region which is not included in these two clusters is very small, and the resulting effect on the morphological fractions is likely minimal.

5.3. Background Subtraction

Galaxies within the magnitude range and distance from the cluster center described in §§ 5.1 and 5.2 lie at a variety of redshifts. We wish to determine the proportions of E, S0, and late-type galaxies among cluster members only. Because the morphological mix of field galaxies differs substantially from that of cluster populations, morphological fractions computed without regard to field contamination will underestimate the fraction of early types and overestimate the fraction of late types in clusters. We use four methods, described in detail below, to account for the presence of cluster nonmembers, checking for consistency among the resulting morphological fractions.

5.3.1. Spectroscopic Redshifts

As described in § 2, the EDisCS program includes an extensive spectroscopic survey. For each cluster, redshifts were obtained for 6–86 galaxies which both meet our apparent magnitude limit and lie within $0.6\,R_{200}$ (*WMAP* cosmology). We use this spectroscopic sample to constrain the morphological fractions in each cluster in two ways. First, we calculate hard limits on the morphological fractions using both the spectroscopic sample and the purely photometric sample, consisting of galaxies that were either not targeted for spectroscopy, or for which spectroscopy failed to yield a red-

shift. This calculation does not require that the spectroscopic sample be complete. Second, we estimate the morphological fractions using only the spectroscopic sample after applying small completeness corrections.

The upper and lower hard limits on the fraction of galaxies of type i are given by:

$$f_{\min}(i) = \frac{N_s^m(i)}{N_s^m + N_p^u - N_p^u(i)} \qquad (4)$$

and

$$f_{\max}(i) = \frac{N_s^m(i) + N_p^u(i)}{N_s^m + N_p^u(i)}, \qquad (5)$$

where the subscripts s and p refer to the spectroscopic sample and the photometric sample, respectively; and the superscripts m and u indicate cluster members and galaxies at unknown (spectroscopic) redshift, respectively. Each quantity is a function of galaxy type i. The fraction of galaxies of type i is minimized when all of the other types that do not have redshifts are members and all of the galaxies of type i that do not have redshifts are nonmembers. The fraction of galaxies of type i is maximized when all of the galaxies of other types without redshifts are nonmembers and all of the galaxies of type i without redshifts are members. The results of applying equations (4) and (5) are shown as the gray shaded regions in Figure 2.

To directly estimate the morphological fractions from the spectroscopic data, we must correct for incompleteness in the spectroscopic sample. As described in the Appendix of Poggianti et al. (2006), the completeness of the EDisCS spectroscopy is a weak function of both apparent I-band magnitude and clustercentric distance. Using the cluster-by-cluster magnitude and geometric completeness weights W_{mag} and W_{geo} calculated in that work, we estimate the spectroscopic morphological fractions $f_{\mathrm{spec}}(i)$ as

$$N_{\mathrm{spec}}(i) = \sum_{j=1}^{N_s^m(i)} W_{\mathrm{mag}}(j)^{-1} W_{\mathrm{geo}}(j)^{-1} \qquad (6)$$

$$N_{\mathrm{spec}}(\mathrm{tot}) = \sum_{j=1}^{N_s^m} W_{\mathrm{mag}}(j)^{-1} W_{\mathrm{geo}}(j)^{-1}. \qquad (7)$$

$$f_{\mathrm{spec}}(i) = N_{\mathrm{spec}}(i)/N_{\mathrm{spec}}(\mathrm{tot}). \qquad (8)$$

The probability of measuring a given morphological fraction is the product of the Poisson probability of measuring the total number of cluster members times the binomial probability of measuring the observed number of a given morphology. We use the approximation presented in equations (21) and (26) of Gehrels (1986) to derive 1 σ error estimates based on this premise, using $N_{\mathrm{spec}}(i)$ and $N_{\mathrm{spec}}(\mathrm{tot})$ as inputs. The results of applying equation (8) are shown as open squares in Figure 2.

As described in § 2, the faint magnitude limit of the EDisCS spectroscopic survey is $I(r = 1'') = 22$ mag for the intermediate-redshift clusters and $I(r = 1'') = 23$ mag for the high-redshift clusters. In general, $I(r = 1'')$ is fainter than I_{auto}. For six of our clusters, all of the galaxies meeting the I_{auto} magnitude and aperture requirements of our analysis have values of $I(r = 1'')$ brighter than the spectroscopic survey limit. However, for cl1054-1245, cl1216-1201, cl1232-1250, and cl1354-1230, 10%–20% are fainter than
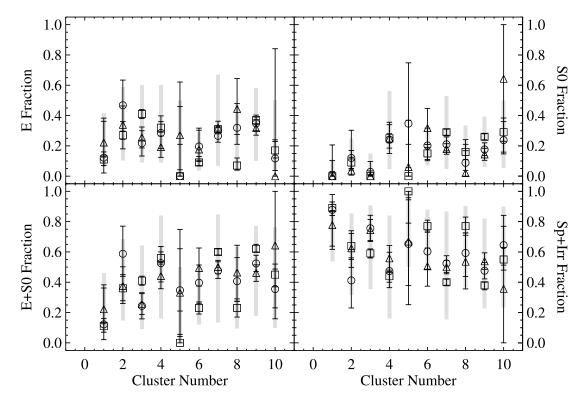
Fig. 2.—Comparison of four methods for estimating the E, S0, E+S0, and Sp+Irr fractions in the 10 EDisCS clusters listed in Table 1. The shaded gray regions span the full range allowed by our spectroscopic data, while the squares show the best estimates of the morphological fractions determined using spectroscopic redshifts (see § 5.3.1). Circles and triangles represent the morphological fractions determined using photometric redshifts (see § 5.3.2) and statistical background subtraction (see § 5.3.3), respectively. All calculations were performed using the *WMAP* cosmology and an aperture of 0.6 R_{200}.

the spectroscopic flux limit. Most ($\gtrsim$80%) of these are late-type galaxies. Thus, it is possible that our direct spectroscopic estimates are biased slightly toward low late-type fractions. In Figure 2, we compare the morphological fractions derived from different methods, and find that for cl1054-1245, cl1216-1201, and cl1232-1250, the spectroscopic method does yield lower late-type fractions than the photometric redshift or statistical background subtraction methods. However, all methods produce late-type fractions that are consistent with one another, within the errors. For cl1354-1230, the spectroscopic method results in a late-type fraction between the photometric redshift method and the statistical background method.

5.3.2. *Photometric Redshifts*

Our optical and near-infrared imaging allows the derivation of photometric redshifts, as described in R. Pelló et al. (2007, in preparation). Briefly, two estimates of the redshift probability distribution [$P(z)$] were computed for each galaxy. Two independent codes were employed, one described in Rudnick et al. (2001) and Rudnick et al. (2003) and `Hyperz`, described in Bolzonella et al. (2000). An estimate of $P(z)$ can be integrated over a suitable interval Δz (in this case ± 0.1) around the cluster redshift to obtain the probability $P_{\rm clust}$ that the galaxy is a member of the cluster. We used our large spectroscopic sample to determine $P_{\rm thresh}$, the minimum value of $P_{\rm clust}$ required for a galaxy to be considered a cluster member. Membership information derived from each of our two estimates of $P(z)$ was then combined to determine cluster membership. That is, both estimates were required to be consistent with cluster membership in order for a galaxy to be considered a cluster member.

We used the subset (vast majority) of our spectroscopic sample with both optical and near-infrared imaging to estimate (1) the

fraction of spectroscopically confirmed cluster members excluded by our photometric redshifts as a function of morphology and (2) the fraction of spectroscopic nonmembers that are photometric members as a function of morphology. Since $P_{\rm thresh}$ was calibrated to include as many cluster members as possible rather than to exclude all nonmembers, the former fraction tends to be significantly smaller than the latter. Given these fractions, we calculated $N_m(i)$, the expected number of cluster members of type i that were missed by the photometric redshifts; and $N_c(i)$, the expected number of nonmembers among galaxies of type i that contaminate the photometric redshift member sample. We then used this information to compute the corrected number of observed cluster members of type i [$N_{\rm photoz}(i)$], and finally, the corrected fraction of cluster members of type i [$f_{\rm photoz}(i)$]:

$$N_{\rm photoz}(i) = N_{\rm obs}(i) + N_m(i) - N_c(i) \qquad (9)$$

$$N_{\rm photoz}(\text{tot}) = N_{\rm photoz}(E) + N_{\rm photoz}(S0) + N_{\rm photoz}(\text{Sp} + \text{Irr}) \quad (10)$$

$$f_{\rm photoz}(i) = N_{\rm photoz}(i)/N_{\rm photoz}(\text{tot}) \qquad (11)$$

As in 5.3.1, errors were computed using the Gehrels (1986) approximation using $N_{\rm photoz}(i)$ and $N_{\rm photoz}(\text{tot})$. The morphological fractions computed using equation (11) are shown as hollow circles in Figure 2.

As described in § 2, the area of each cluster with near-infrared imaging is somewhat smaller than that imaged in the optical. In the classic cosmology, an analysis radius of 600 kpc extends beyond the near-infrared imaging for cl1227-1138. As a result, 19 out of 49 galaxies meeting the magnitude and aperture requirements for inclusion in the morphological analysis lack near-infrared data.

TABLE 3
Morphological Fractions within EDisCS Clusters

Cluster Number	f_E	f_{S0}	f_{E+S0}	f_{Sp+Irr}	f_{Sp}	f_{Irr}
cl1037..................	$0.281^{+0.124}_{-0.146}$	$0.000^{+0.109}_{-0.000}$	$0.281^{+0.124}_{-0.124}$	$0.719^{+0.146}_{-0.124}$	$0.625^{+0.138}_{-0.156}$	$0.095^{+0.174}_{-0.050}$
cl1040..................	$0.377^{+0.136}_{-0.116}$	$0.066^{+0.093}_{-0.058}$	$0.444^{+0.141}_{-0.123}$	$0.556^{+0.123}_{-0.141}$	$0.419^{+0.141}_{-0.115}$	$0.137^{+0.127}_{-0.071}$
cl1054-11..............	$0.245^{+0.071}_{-0.069}$	$0.000^{+0.036}_{-0.000}$	$0.245^{+0.071}_{-0.069}$	$0.755^{+0.069}_{-0.071}$	$0.755^{+0.069}_{-0.071}$	$0.000^{+0.036}_{-0.000}$
cl1054-12	$0.300^{+0.107}_{-0.090}$	$0.267^{+0.104}_{-0.087}$	$0.567^{+0.102}_{-0.102}$	$0.433^{+0.108}_{-0.108}$	$0.433^{+0.108}_{-0.102}$	$0.000^{+0.060}_{-0.000}$
cl1103..................	$0.250^{+0.120}_{-0.080}$	$0.000^{+0.070}_{-0.000}$	$0.250^{+0.120}_{-0.120}$	$0.750^{+0.080}_{-0.120}$	$0.750^{+0.080}_{-0.120}$	$0.000^{+0.070}_{-0.000}$
cl1138..................	$0.305^{+0.164}_{-0.120}$	$0.095^{+0.113}_{-0.084}$	$0.400^{+0.162}_{-0.145}$	$0.600^{+0.145}_{-0.162}$	$0.600^{+0.145}_{-0.162}$	$0.000^{+0.115}_{-0.000}$
cl1216..................	$0.490^{+0.030}_{-0.020}$	$0.220^{+0.020}_{-0.020}$	$0.710^{+0.020}_{-0.020}$	$0.290^{+0.020}_{-0.020}$	$0.270^{+0.020}_{-0.020}$	$0.020^{+0.010}_{-0.010}$
cl1227..................	$0.290^{+0.165}_{-0.136}$	$0.146^{+0.157}_{-0.095}$	$0.436^{+0.160}_{-0.162}$	$0.564^{+0.162}_{-0.160}$	$0.394^{+0.167}_{-0.164}$	$0.170^{+0.132}_{-0.120}$
cl1232..................	$0.350^{+0.040}_{-0.040}$	$0.170^{+0.030}_{-0.030}$	$0.530^{+0.040}_{-0.040}$	$0.470^{+0.040}_{-0.040}$	$0.470^{+0.040}_{-0.040}$	$0.000^{+0.010}_{-0.000}$
cl1354..................	$0.170^{+0.070}_{-0.050}$	$0.290^{+0.070}_{-0.060}$	$0.450^{+0.070}_{-0.080}$	$0.550^{+0.080}_{-0.070}$	$0.550^{+0.080}_{-0.070}$	$0.000^{+0.030}_{-0.000}$

Notes.—$R = 600$ kpc, $\Omega_0 = 1$, $\Lambda = 0$, $H_0 = 50$ km s^{-1} Mpc^{-1}. The morphological fractions for a given cluster were computed using the background subtraction method adopted for that cluster (see § 6).

Using the *WMAP* cosmology and an analysis radius of 0.6 R_{200}, a similar problem occurs for both cl1227-1138 (21 out of 50 galaxies lack near-infrared data) and cl1232-1250 (14 out of 222 galaxies lack near-infrared data). Because the $P(z)$ distributions for photometric redshifts computed without near-infrared data are broad, they have low P_{clust} values and are somewhat more likely to be rejected than galaxies with photometric redshifts computed using the full filter set. Figure 2 shows that this effect does not appear to have systematically skewed the morphological fractions for cl1227-1138 and cl1232-1250 compared to the other methods employed.

5.3.3. Statistical Background Subtraction

In the absence of spectroscopic or photometric redshift information for each galaxy, we can still estimate the morphological fractions by statistically correcting the number of observed galaxies of a given type to account for sources that lie in the field:

$$N_{field} = \Sigma_{field} A, \quad (12)$$

$$N_{stat}(i) = N_{obs}(i) - N_{field} P(i) \quad (13)$$

$$N_{stat}(tot) = N_{obs}(tot) - N_{field} \quad (14)$$

$$f_{stat}(i) = N_{stat}(i)/N_{stat}(tot). \quad (15)$$

Here A is the area of the aperture described in § 5.2; $N_{obs}(tot)$ is the total number of galaxies meeting the magnitude criterion (§ 5.1) within that aperture; $N_{obs}(i)$ is the number of these galaxies which have morphology i; N_{field} is the number of the observed galaxies that are expected to be field members; and $N_{stat}(tot)$ and $N_{stat}(i)$ are the background-subtracted number of galaxies in the aperture and the number of type i, respectively. The surface density of field galaxies, Σ_{field}, is determined by integrating the I-band differential number counts in Table 1 of Postman et al. (1998) down to the redshift-dependent I-band apparent magnitude limit adopted for each cluster, as described in § 5.1. We computed $P(i)$, the fraction of field galaxies of each morphological type, using data from the Medium Deep Survey (MDS; Griffiths et al. 1994), a Hubble Telescope Key Project that cataloged the morphologies of intermediate-redshift field galaxies down to $I_{814} \sim 22$ mag. In particular, we used the classifications of Richard Ellis listed in Table 1 of Abraham et al. (1996). The magnitude limits, $I_{auto,lim}$, of our morphological analysis vary from cluster to cluster and with cosmology but generally range from 21.3 to 23 mag. The values of $P(i)$ are a function of $I_{auto,lim}$, decreasing to faint magnitudes for

early-type galaxies and increasing to faint magnitudes for late types. For those clusters with $I_{auto,lim} > 22$ mag, we adopt the values of $P(i)$ down to $I_{814} = 22$ mag. Based on the behavior of $P(i)$ versus I_{814}, this procedure likely overestimates $P(E)$, $P(S0)$, and $P(Sp)$ and underestimates $P(Sp + Irr)$ and $P(Irr)$. These trends translate into underestimates of the E, S0, and Sp morphological fractions and overestimates of the Sp+Irr and Irr fractions. These misestimates will be most severe for cl1054-1245, cl1216-1201, and cl1354-1230, which have the faintest values of $I_{auto,lim}$. The morphological fractions computed using statistical background subtraction and equation (15) are shown as open triangles in Figure 2. Examination of this figure does not reveal any obvious biases with respect to other methods that could be attributable to our $P(i)$ estimates.

As in §§ 5.3.1 and 5.3.2, errors were computed using the Gehrels (1986) approximation and $N_{stat}(i)$ and $N_{stat}(tot)$.

6. RESULTS

We have estimated the morphological fractions of 10 EDisCS clusters at $0.5 < z < 0.8$ using four different background-subtraction techniques (absolute limits from spectroscopic redshifts, direct estimates from spectroscopic redshifts, photometric redshifts, and statistical subtraction), within apertures of different radii (600 kpc and 0.6 R_{200}), and for two different cosmologies (the classic cosmology: $\Omega_0 = 1$, $\Lambda = 0$, $H_0 = 50$ km s^{-1} Mpc^{-1}; and the *WMAP* cosmology: $\Omega_0 = 0.3$, $\Lambda = 0.7$, $H_0 = 70$ km s^{-1} Mpc^{-1}). Figure 2 shows how the different methods compare for an aperture of 0.6 R_{200} in the *WMAP* cosmology. The direct estimate methods are consistent with the absolute limits derived from our spectroscopy, and with one another. In addition, there is no systematic trend for one estimate to produce higher or lower fractions than any other. For each cluster we therefore adopt a single method: direct estimate from spectroscopy, photometric redshifts, or statistical background subtraction. The adopted method, which differs from cluster to cluster, is chosen in the following way. For a given cluster, median E, S0, and Sp+Irr fractions are selected from among the estimates of all three methods. The method selected most often in this process is the one adopted for the cluster. The E, S0, and Sp+Irr fractions estimated using the chosen method for each cluster are shown in Tables 3 and 4, and are the quantities plotted in Figures 3 through 5.

The morphological fractions in Figure 2 appear to be correlated with cluster number, which is determined by right ascension. Spearman and Kendall rank correlation tests show that marginal correlations are detected at the $\sim$2 σ level for the S0 and Sp+Irr fractions. We find no correlation between cluster redshift and

TABLE 4
MORPHOLOGICAL FRACTIONS WITHIN EDisCS CLUSTERS

Cluster Number	E	S0	E+S0	$f_{\rm Sp+Irr}$	$f_{\rm Sp}$	$f_{\rm Irr}$
cl1037..................	$0.122^{+0.240}_{-0.101}$	$0.000^{+0.206}_{-0.000}$	$0.122^{+0.240}_{-0.101}$	$0.878^{+0.101}_{-0.240}$	$0.854^{+0.124}_{-0.217}$	$0.023^{+0.182}_{-0.023}$
cl1040..................	$0.339^{+0.124}_{-0.096}$	$0.037^{+0.088}_{-0.030}$	$0.376^{+0.126}_{-0.098}$	$0.624^{+0.098}_{-0.126}$	$0.624^{+0.098}_{-0.126}$	$0.000^{+0.068}_{-0.000}$
cl1054-11..............	$0.256^{+0.069}_{-0.069}$	$0.000^{+0.035}_{-0.000}$	$0.256^{+0.069}_{-0.069}$	$0.744^{+0.069}_{-0.069}$	$0.744^{+0.069}_{-0.069}$	$0.000^{+0.035}_{-0.000}$
cl1054-12	$0.285^{+0.113}_{-0.102}$	$0.241^{+0.115}_{-0.092}$	$0.526^{+0.110}_{-0.124}$	$0.474^{+0.124}_{-0.110}$	$0.469^{+0.108}_{-0.120}$	$0.005^{+0.066}_{-0.005}$
cl1103..................	$0.271^{+0.350}_{-0.229}$	$0.060^{+0.309}_{-0.060}$	$0.331^{+0.290}_{-0.289}$	$0.669^{+0.289}_{-0.290}$	$0.669^{+0.289}_{-0.290}$	$0.000^{+0.369}_{-0.000}$
cl1138..................	$0.196^{+0.121}_{-0.094}$	$0.202^{+0.115}_{-0.100}$	$0.397^{+0.117}_{-0.136}$	$0.603^{+0.136}_{-0.117}$	$0.603^{+0.136}_{-0.117}$	$0.000^{+0.084}_{-0.000}$
cl1216..................	$0.266^{+0.056}_{-0.042}$	$0.210^{+0.049}_{-0.043}$	$0.476^{+0.059}_{-0.051}$	$0.524^{+0.051}_{-0.059}$	$0.432^{+0.053}_{-0.055}$	$0.092^{+0.036}_{-0.031}$
cl1227..................	$0.319^{+0.160}_{-0.109}$	$0.088^{+0.153}_{-0.049}$	$0.407^{+0.155}_{-0.133}$	$0.593^{+0.133}_{-0.155}$	$0.494^{+0.146}_{-0.135}$	$0.099^{+0.142}_{-0.059}$
cl1232..................	$0.348^{+0.055}_{-0.048}$	$0.176^{+0.044}_{-0.040}$	$0.524^{+0.054}_{-0.054}$	$0.476^{+0.054}_{-0.054}$	$0.425^{+0.052}_{-0.054}$	$0.051^{+0.029}_{-0.024}$
cl1354..................	$0.170^{+0.070}_{-0.050}$	$0.290^{+0.070}_{-0.060}$	$0.450^{+0.070}_{-0.080}$	$0.550^{+0.080}_{-0.070}$	$0.550^{+0.080}_{-0.070}$	$0.000^{+0.030}_{-0.000}$

NOTES.—$R = 0.6\,R_{200}$, $\Omega_0 = 0.3$, $\Lambda = 0.7$, $H_0 = 70$ km s^{-1} Mpc^{-1}. The morphological fractions for a given cluster were computed using the background subtraction method adopted for that cluster (see § 6).

cluster number that could explain this trend. However, we find that the cluster velocity dispersion is correlated with the cluster number, also at the $\sim 2\,\sigma$ level. Since there is no reason for any physical property of the cluster to correlate with cluster number, these correlations hint that the morphological fractions correlate with cluster velocity dispersion, a possibility we revisit in § 6.2.

6.1. *Evolution of Cluster Morphological Content*

To assess the degree of evolution in the morphological content of rich clusters, we searched the literature for similar analyses of clusters spanning a broad redshift range. The first comparison sample consists of $z < 0.5$ clusters with morphological fractions originally measured by different groups using a variety of methods, but

reanalyzed in a uniform manner by Fasano et al. (2000, hereafter F00). The F00 sample includes 55 low-redshift clusters (Dressler 1980a; Dressler et al. 1997); the 10 MORPHS clusters at $0.37 < z < 0.5$ (Dressler et al. 1997); three clusters at $z \sim 0.3$ plus A2218 and A1689 at $z = 0.18$ (Couch et al. 1998); and nine clusters at $0.1 < z < 0.25$ (Fasano et al. 2000). Using this large sample of uniformly analyzed clusters at $z < 0.5$, Fasano et al. (2000) confirmed the MORPHs finding that the S0 fraction in clusters has doubled since $z \sim 0.5$, while the late-type fraction has decreased by a similar factor.

We also compare our results with that of Postman et al. (2005, hereafter P05). They computed the morphological fractions within the virial radii of seven clusters at $0.8 < z < 1.27$. This is the only
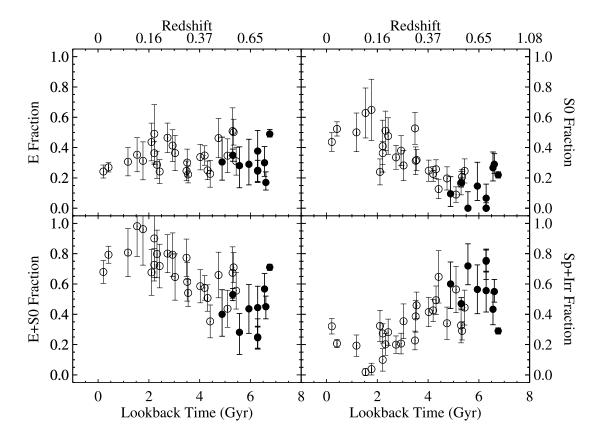

FIG. 3.—Evolution of the E, S0, E+S0, and Sp+Irr fractions as traced by EDisCS clusters (*filled circles*) and F00 clusters (*open circles*). All fractions were computed within a radius of 600 kpc, using the classic cosmology. The lookback times were calculated with the *WMAP* cosmology.
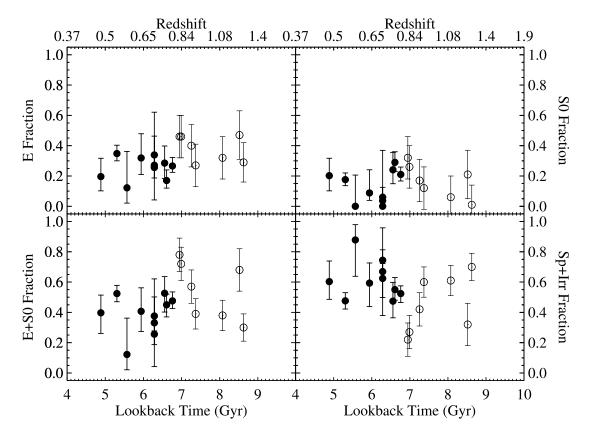
Fig. 4.—Evolution of the E, S0, E+S0, and Sp+Irr fractions as traced by EDisCS clusters (*filled circles*) and P05 clusters (*open circles*). The EDisCS fractions were computed within a radius of 0.6 R_{200} and the P05 fractions were computed within a radius of R_{200}. All computations were performed using the *WMAP* cosmology.

large study of clusters at these redshifts in which S0 galaxies are separately classified. As previously discussed, the S0 population is an important one to track at high redshift.

In Figure 3, we show the evolution at $z < 0.8$ of the morphological fractions in rich clusters, using EDisCS data in conjunction with the F00 sample described above. All points were computed within 600 kpc, using the classic cosmology. We do not include measurements made on the Postman sample in this plot because they were computed within R_{200} using the *WMAP* cosmology. As discussed previously, the F00 sample shows a systematic decrease in the S0 fraction from 55% at $z = 0$ to 20% at $z \sim 0.5$. Where the redshift range of the EDisCS clusters overlaps with that of F00, the morphological fractions derived from the two samples are generally consistent. However, the longer redshift baseline afforded by the addition of the EDisCS data reveals that the S0 fraction is actually flat over the range $0.4 < z < 0.8$. This could mean that $z \sim 0.4$ is a special epoch after which the S0 fraction in cluster cores begins to grow. The coincidence of this special epoch with the redshift where the two samples overlap raises the question of whether the samples were analyzed in different ways. However, § 5 describes our extensive attempts to control systematics in the EDisCS sample and to conform to the analysis presented by F00. Alternatively, it is possible that we are missing some S0-rich clusters at $z \sim 0.4$, which would reveal that the growth of the S0 fraction in clusters at $z < 0.4$ is slower than suggested by the present data. Indeed, the scatter in the morphological fractions at $z \sim 0.4$ is smaller than at either higher or lower redshifts.

The F00+EDisCS data are consistent with either a bend in the morphological fractions at $z \sim 0.4$ or a smooth continuation of the trends observed at $z < 0.5$, but with a flatter overall slope than suggested by the F00 data alone. More observations at $z \sim 0.4$

and $z > 0.8$ are required to distinguish between these two possibilities. As discussed above, P05 have analyzed the morphological fractions, including the S0 fraction, in clusters at $z > 0.8$. In Figure 4 we show the morphological fractions of the EDisCS and P05 clusters as functions of redshift. All estimates were made using the WMAP cosmology, but the EDisCS fractions were computed within 0.6 R_{200} (see § 5.2), while the P05 fractions were computed within R_{200}. P05 find that the E and E+S0 fractions decrease out to 0.6 R_{200}, while the S0 fraction stays roughly constant and the Sp+Irr fraction increases. Between 0.6 R_{200} and R_{200}, all the fractions are flat. According to Table 4 of P05, the E, S0, early-, and late-type fractions computed within R_{200} are factors of approximately 0.79, 0.96, 0.85, and 1.15 times the fractions computed within 0.6 R_{200}. However, no corrections have been made to the points shown in Figure 4.

Figure 4 shows that the strong evolution in morphological fractions seen at $z < 0.4$ does not continue at $z > 0.4$. Indeed, the E+S0 (Sp+Irr) fraction appears to be larger (smaller) in the higher redshift P05 sample compared to the EDisCS clusters. However, a Spearman rank correlation analysis shows that there is no statistically significant evidence for any evolution over the entire redshift interval $0.4 < z < 1.25$, or in the individual EDisCS and P05 samples. Additional clusters in this redshift range are necessary to reveal the presence of any weak correlation.

How does the selection requirement for the EDisCS clusters to exhibit a red sequence affect the interpretation of Figures 3 and 4? If the red sequence takes time to build up, it may be expected that this requirement selects for clusters that are also dynamically evolved. In fact, the EDisCS sample includes clusters that are clearly nonspherical, as well as clusters that display significant substructure (see § 6.2). The red sequence requirement may also
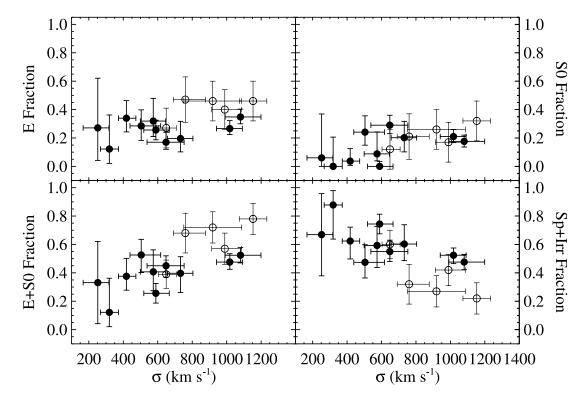
FIG. 5.—Morphological fractions as a function of cluster velocity dispersion for the EDisCS clusters (*filled circles*) and the subset of the P05 cluster sample for which velocity dispersions are available (*open circles*). The EDisCS fractions were computed within a radius of 0.6 R_{200} and the P05 fractions were computed within a radius of R_{200}. All fractions were computed using the *WMAP* cosmology.

be expected to select for clusters with high E and/or S0 fractions. Figure 3 demonstrates that the EDisCS clusters do not contain large E fractions compared to either the optically selected F00 sample at lower redshifts or the (primarily) X-ray–selected P05 sample at higher redshifts. Thus, either such a bias is weak, or it is shared by the comparison samples. Given the correlation between galaxy color and morphology, any clusters lacking a red sequence would likely have significantly different morphological fractions from the EDisCS, F00, and P05 samples, leading to increased scatter in Figures 3 and 4. While both the incidence of such clusters and their morphological content are currently impossible to quantify, in the next subsection we evaluate the dependence of morphological fractions on another cluster property: velocity dispersion.

6.2. *Correlation between Morphological Fractions and Cluster Velocity Dispersion*

In the previous subsection we argued that there is no systematic evolution in the morphological fractions within rich clusters at $0.4 < z < 1.25$. Figures 3 and 4 indicate that the scatter in these fractions is large. How much of this scatter is due to a correlation between morphological fractions and cluster mass? Such a correlation may be expected in either nature or nurture scenarios. In the former it is due to the fact that the most massive clusters collapsed at earlier times. In the latter it could be due to a higher efficiency of morphological transformations in more massive clusters.

P05 found that the E, S0, and E+S0 fractions within R_{200} of seven $z \sim 1$ clusters increase with increasing bolometric cluster X-ray luminosity, although the correlations are significant only at the $\lesssim 3\,\sigma$ level. However, they find no correlation between the E+S0 fraction and the X-ray temperature or the cluster velocity dispersion, perhaps because of small number statistics. In Fig-

ure 5 we plot the morphological fractions of the EDisCS and P05 samples against cluster velocity dispersion. From this figure it is apparent that clusters with larger velocity dispersions harbor a higher fraction of early type galaxies and fewer late type galaxies. Spearman and Kendall rank correlation tests show that these visual impressions are statistically significant at the $\lesssim 3\,\sigma$ level.

While it is tempting to interpret this correlation as one between morphological content and cluster mass, the velocity dispersion of a cluster is directly related to its mass only if the cluster is virialized. The velocity dispersion may overpredict mass if the cluster is experiencing significant merging events. The degree of substructure in five of the clusters in this work (cl1040-1155, cl1054-1146, cl1054-1245, cl1216-1201, and cl1232-1250) has been studied in detail by Halliday et al. (2004) using Dressler-Shectman tests (Dressler & Shectman 1988). They detect substructure in cl1232-1250 and cl1216-1201 with more than 95% confidence. For cl1040-1155 and cl1054-1245, not enough spectra were available to provide firm evidence for substructure. No evidence for substructure was found for cl1054-1146. They note that the two clusters showing clear evidence of substructure also have the largest velocity dispersions in the EDisCS sample, and caution against using the velocity dispersions for these two clusters as a proxy for mass. Further analysis on the remaining EDisCS clusters is ongoing (B. Milvang-Jensen et al. 2007, in preparation).

What is the situation for the $z < 0.5$ sample, where evolution is observed? Velocity dispersions were available in the literature for 14 of the clusters in the F00 sample (Couch & Sharples 1987; Gudehus 1989; Girardi & Mezzetti 2001; De Propris et al. 2002; Bettoni et al. 2006). Figure 6 shows the morphological fractions for these 14 F00 clusters as a function of cluster velocity dispersion. Without a larger number of data points it is difficult to make a conclusive statement regarding the existence of a correlation. Spearman and Kendall rank correlation tests indicate that none
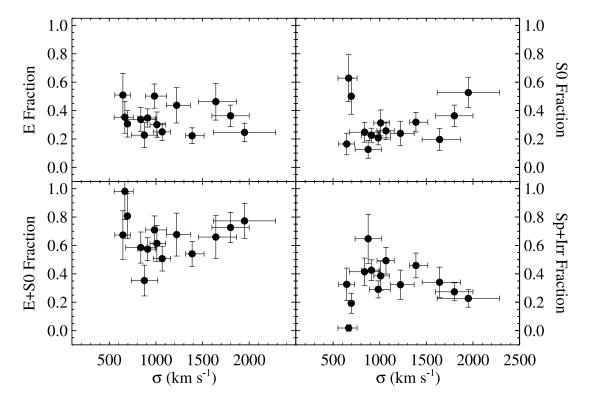
Fig. 6.—Same as Fig. 5, but for the subset of the F00 cluster sample for which velocity dispersions are available. All morphological fractions were computed within 600 kpc using the classic cosmology. The velocity dispersion measurements for 10 of these clusters come from Girardi & Mezzetti (2001). The remainder come from Bettoni et al. (2006; A3330 with $\sigma = 695$ km s^{-1}), De Propris et al. (2002; A389 with $\sigma = 667$ km s^{-1}), Gudehus (1989; A1689 with $\sigma = 1800$ km s^{-1}), and Couch & Sharples (1987; AC118 with $\sigma = 1950$ km s^{-1}). Both A3330 and A389 have large S0 fractions compared to other clusters with similar velocity dispersions. In addition, A1689 and AC118 are the F00 clusters with the largest velocity dispersions, and largely drive the correlation between morphological fractions and velocity dispersion. This plot illustrates the need for homogeneous studies of velocity dispersions for clusters where evolution in morphological fractions is observed.
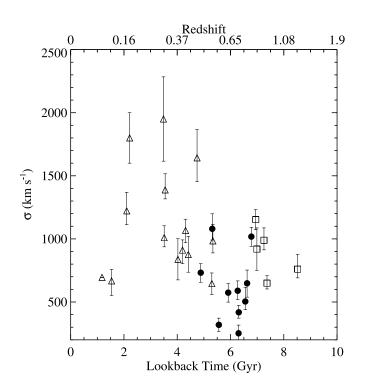

Fig. 7.—Cluster velocity dispersion as a function of cluster lookback time for the EDisCS sample (*filled circles*), the subset of the F00 sample for which velocity dispersions were available (*open triangles*), and the subset of the P05 sample for which velocity dispersions were available (*open squares*). The lookback time was calculated using the *WMAP* cosmology.

of the morphological fractions are significantly correlated with cluster velocity dispersion. However, removal of two clusters (A389 and A3330) with unusually high S0 fractions for their velocity dispersions results in a 2 σ detection of a correlation between S0 fraction and cluster velocity dispersion. Additional velocity dispersions for the F00 sample would greatly aid an assessment of any correlation, which is necessary for understanding the observed trends between morphology and redshift.

Comparing the *x*-axes of Figures 5 and 6, we see that the F00 sample at $z < 0.5$ includes some clusters with very high velocity dispersions ($\sigma > 1200$ km s^{-1}), while the $z > 0.5$ EDisCS+P05 sample does not. Figure 7 shows the cluster velocity dispersions of the EDisCS, F00, and P05 samples as a function of lookback time. The clusters with the highest velocity dispersions in these samples lie at low redshift. Unfortunately, velocity dispersions are unavailable for a significant fraction of the low-redshift sample. These are urgently needed to understand the extent to which sample selection is responsible for the apparent evolution in the morphological content of clusters.

7. DISCUSSION AND CONCLUSIONS

Using high-resolution imaging afforded by the ACS instrument on board the *Hubble Space Telescope*, we find no evidence for evolution in the morphological content of rich clusters with velocity dispersions in the range $\sigma = 200$–1200 km s^{-1} over the redshift range $0.4 < z < 1.25$ (see Figs. 3 and 4). Although the scatter is significant, typical morphological fractions for clusters in this redshift range are 0.3, 0.15, and 0.55 for E, S0, and Sp+Irr galaxies, respectively. In contrast, studies of clusters at lower redshifts have shown that the elliptical fraction remains constant between $z = 0$ and $z \sim 0.5$, while the S0 fraction decreases by a

factor of ~ 2 and the Sp+Irr fraction increases by a similar amount over the same redshift range (e.g., F00). Our data show that the observed evolution in cluster S0 and Sp+Irr populations does not continue beyond $z \sim 0.4$, at least for the velocity dispersions probed in this study.

How do our results concerning the global evolution of galaxy morphologies within rich clusters translate into a statement regarding the evolution of the morphology-density relation? Although the centers of cluster cores are regions of high local galaxy density, our morphological fractions were computed within sizable apertures (see § 5.2), so the average environment we are probing is of moderate density. For example, the average galaxy surface density within a radius of 0.6 R_{200} ($\Omega_0 = 0.3$, $\Lambda = 0.7$, $H_0 = 70$ km s^{-1} Mpc^{-1}) for the EDisCS clusters used in this analysis ranges from ~ 40–175 Mpc^{-2}. The morphological fractions of the F00 and P05 clusters were likely computed using galaxies inhabiting environments of similar average density. These results may point to a lack of evolution in the morphology density relation between $z = 0.8$ and 0.4, with a subsequent increase in the S0 population and a decrease in the Sp+Irr population. Larger samples in this redshift range are needed to understand the scatter in the morphological fractions, and to rule out weak evolution. However, our current data are consistent with recent studies of the morphology-density relation at $z \sim 1$ (Smith et al. 2005; Postman et al. 2005).

Several studies of nearby galaxies indicate that the observed relation between morphology and environment is a reflection of a more primary relation between star formation rate (SFR) and environment (Kauffmann et al. 2004; Christlein & Zabludoff 2005; Blanton et al. 2005). The star formation properties of cluster, group, and field galaxies in the EDisCS spectroscopic sample have been measured and compared to a low-redshift sample from the Sloan Digital Sky Survey by Poggianti et al. (2006, hereafter P06). Based on these data, P06 put forth a model in which passive galaxies devoid of ongoing star formation are made up of two separate populations: "primordial" galaxies whose stars all formed at $z > 2.5$ and galaxies whose star formation lasted until later times but was ultimately "quenched" due to entering a cluster-like environment ($>10^{14}$ $M_\odot$). In this model the primordial galaxies may be identified with the elliptical galaxies that make up $\sim 30\%$ on average of the galaxy populations in clusters at $z < 1$, and perhaps some of the S0 galaxies (see below). This identification is consistent with both the lack of evolution in the elliptical fraction at $z < 1$ and with the old ages inferred for elliptical stellar populations. It is tempting to identify the quenched galaxies with S0's. However, the fraction of quenched galaxies in the model increases at $z < 0.8$, while the S0 fraction only increases at $z < 0.4$. These timescales are consistent if it takes roughly a billion years for a galaxy to resemble an S0 after the cessation of star formation in a spiral galaxy (Dressler et al. 1999; Poggianti et al. 1999; Tran et al. 2003). However, the formation of the S0 population observed in clusters at $0.4 < z < 1$ cannot be explained in this way. Perhaps these are primordial S0's that assumed an S0 morphology upon or soon after formation at $z > 2.5$. If so, the S0 galaxies in clusters at $z > 0.4$ should be, on average, older and more massive than cluster S0's at $z < 0.4$. Another possibility is that at least some late types may transform into S0's in systems less massive than 10^{14} $M_\odot$, perhaps by an entirely different mechanism than operates in $>10^{14}$ $M_\odot$ systems. The existence of S0's in groups (e.g., Hickson et al. 1989) suggests that this may be the case.

If a significant fraction of S0 galaxies in nearby clusters were quenched, what did they look like beforehand? The parallel decline in the Sp+Irr fraction as the S0 fraction increases between $z = 0.4$ and 0 suggests that some subset of late-type galaxies transformed into S0's subsequent to quenching. For the EDisCS clusters, we computed the fractions of Sp and Irr galaxies separately (see Tables 3 through 4). As with the other morphological fractions at $z > 0.4$, the Sp and Irr fractions do not vary systematically with redshift. Moreover, the Irr fractions in the EDisCS clusters are very small. We conclude that Sp galaxies and not Irr galaxies are the precursors of the quenched S0's in local clusters.

In the P06 model, both nature and nurture (within clusters) play a role in the environmental dependence of star formation and therefore morphology. The nurture component within clusters is consistent with the observation that the relation between star formation and environment in nearby clusters is not solely a reflection of the relation between stellar age and environment, as would be expected in a pure nature scenario (Christlein & Zabludoff 2005). The P06 model is also compatible with observations which show that the SFR-density relation out to $z \sim 1$ extends to very low local densities, comparable to those found at the virial radius of clusters and even outside clusters (Lewis et al. 2002; Gómez et al. 2003; Cooper et al. 2006). The low-density relations could be set up by the dependence of galaxy properties on initial conditions, or perhaps a different mechanism creates S0 galaxies in low-density environments, or a combination of factors could be responsible.

Although the model forwarded by P06 is an attractive framework within which to view our observational results on the morphological content of rich clusters, it is not necessarily the only model that could explain all of the data accumulating on the evolution of galaxy properties with environment. Furthermore, it does not identify a mechanism responsible for the quenching, although it does specify a timescale (3 Gyr) and a mass scale (10^{14} $M_\odot$) of a workable mechanism.

In addition to analyzing the evolution of the morphological content in galaxy clusters out to $z = 1.25$, we have also studied the dependence of the morphological content on the cluster velocity dispersion (see Figs. 5 and 6). We find that the early- and late-type fractions in the EDisCS and P05 cluster samples correlate with cluster velocity dispersion at a statistically significant level. This correlation highlights the importance of understanding global cluster properties in samples where evolution is observed, such as the F00 sample. Unfortunately, only limited velocity dispersion information is available for the F00 clusters. The existing information for 14 clusters indicates that they have a higher average velocity dispersion than either the EDisCS or P05 clusters. In addition, the morphological fractions of these 14 clusters do not correlate strongly with cluster velocity dispersion. It is possible that additional velocity dispersions for the F00 sample will reveal an underlying trend, that additional studies at high redshift will prove the trend observed in the higher redshift EDisCS+P05 sample to be spurious, or that the relation between morphological fraction and cluster velocity dispersion is itself a function of redshift. Larger cluster samples with robust velocity dispersions and morphologies are needed to determine which of these options is most likely. If the morphology-density relation is driven by environmental processes in clusters, such measurements are essential for determining how the efficiency of these transformations depends on cluster velocity dispersion, which, as discussed in § 6.2, is related to both the cluster mass and its dynamical state.

REFERENCES

Abadi, M. G., Moore, B., & Bower, R. G. 1999, MNRAS, 308, 947
Abraham, R. G., Tanvir, N. R., Santiago, B. X., Ellis, R. S., Glazebrook, K., & van den Bergh, S. 1996, MNRAS, 279, L47
Bekki, K., Couch, W. J., & Shioya, Y. 2002, ApJ, 577, 651
Bertin, E., & Arnouts, S. 1996, A&AS, 117, 393
Bettoni, D., Moles, M., Kjærgaard, P., Fasano, G., & Varela, J. 2006, A&A, 452, 811
Blanton, M. R., Eisenstein, D., Hogg, D. W., Schlegel, D. J., & Brinkmann, J. 2005, ApJ, 629, 143
Blanton, M. R., et al. 2001, AJ, 121, 2358
Bolzonella, M., Miralles, J.-M., & Pelló, R. 2000, A&A, 363, 476
Byrd, G., & Valtonen, M. 1990, ApJ, 350, 89
Christlein, D., & Zabludoff, A. I. 2005, ApJ, 621, 201
Clowe, D., et al. 2006, A&A, 451, 395
Cooper, M. C., et al. 2006, MNRAS, 370, 198
Couch, W. J., Barger, A. J., Smail, I., Ellis, R. S., & Sharples, R. M. 1998, ApJ, 497, 188
Couch, W. J., & Sharples, R. M. 1987, MNRAS, 229, 423
Dalcanton, J. J. 1996, ApJ, 466, 92
De Propris, R., et al. 2002, MNRAS, 329, 87
Dressler, A. 1980a, ApJS, 42, 565
———. 1980b, ApJ, 236, 351
Dressler, A., & Shectman, S. A. 1988, AJ, 95, 985
Dressler, A., Smail, I., Poggianti, B. M., Butcher, H., Couch, W. J., Ellis, R. S., & Oemler, A. J. 1999, ApJS, 122, 51
Dressler, A., et al. 1997, ApJ, 490, 577
Fasano, G., Poggianti, B. M., Couch, W. J., Bettoni, D., Kjærgaard, P., & Moles, M. 2000, ApJ, 542, 673
Finn, R. A., et al. 2005, ApJ, 630, 206
Gehrels, N. 1986, ApJ, 303, 336
Girardi, M., & Mezzetti, M. 2001, ApJ, 548, 79
Gómez, P. L., et al. 2003, ApJ, 584, 210
Gonzalez, A. H., Zaritsky, D., Dalcanton, J. J., & Nelson, A. 2001, ApJS, 137, 117
Goto, T., Yagi, M., Tanaka, M., & Okamura, S. 2004, MNRAS, 348, 515
Goto, T., et al. 2002, PASJ, 54, 515
Griffiths, R. E., et al. 1994, ApJ, 435, L19
Gudehus, D. H. 1989, ApJ, 340, 661

Gunn, J. E., & Gott, J. R. I. 1972, ApJ, 176, 1
Halliday, C., et al. 2004, A&A, 427, 397
Hickson, P., Kindl, E., & Auman, J. R. 1989, ApJS, 70, 687
Icke, V. 1985, A&A, 144, 115
Kauffmann, G., White, S. D. M., Heckman, T. M., Ménard, B., Brinchmann, J., Charlot, S., Tremonti, C., & Brinkmann, J. 2004, MNRAS, 353, 713
Larson, R. B., Tinsley, B. M., & Caldwell, C. N. 1980, ApJ, 237, 692
Lavery, R. J., & Henry, J. P. 1988, ApJ, 330, 596
Lewis, I., et al. 2002, MNRAS, 334, 673
Melnick, J., & Sargent, W. L. W. 1977, ApJ, 215, 401
Mihos, J. C. 2004, in Clusters of Galaxies: Probes of Cosmological Structure and Galaxy Evolution, ed. J. S. Mulchaey, A. Dressler, & A. Oemler (Cambridge: Cambridge Univ. Press), 277
Moore, B., Lake, G., & Katz, N. 1998, ApJ, 495, 139
Poggianti, B. M. 1997, A&AS, 122, 399
Poggianti, B. M., Smail, I., Dressler, A., Couch, W. J., Barger, A. J., Butcher, H., Ellis, R. S., & Oemler, A. J. 1999, ApJ, 518, 576
Poggianti, B. M., et al. 2006, ApJ, 642, 188
Postman, M., Lauer, T. R., Szapudi, I., & Oegerle, W. 1998, ApJ, 506, 33
Postman, M., et al. 2005, ApJ, 623, 721
Quilis, V., Moore, B., & Bower, R. 2000, Science, 288, 1617
Richstone, D. O. 1976, ApJ, 204, 642
Rudnick, G., et al. 2001, AJ, 122, 2205
———. 2003, ApJ, 599, 847
Smail, I., Dressler, A., Couch, W. J., Ellis, R. S., Oemler, A. J., Butcher, H., & Sharples, R. M. 1997, ApJS, 110, 213
Smith, G. P., Treu, T., Ellis, R. S., Moran, S. M., & Dressler, A. 2005, ApJ, 620, 78
Thomas, T., & Katgert, P. 2006, A&A, 446, 31
Toomre, A., & Toomre, J. 1972, ApJ, 178, 623
Tran, K. H., Simard, L., Illingworth, G., & Franx, M. 2003, ApJ, 590, 238
Treu, T., Ellis, R. S., Kneib, J., Dressler, A., Smail, I., Czoske, O., Oemler, A., & Natarajan, P. 2003, ApJ, 591, 53
White, S. D. M., et al. 2005, A&A, 444, 365
Zaritsky, D., Nelson, A. E., Dalcanton, J. J., & Gonzalez, A. H. 1997, ApJ, 480, L91
Zucca, E., et al. 2006, A&A, 455, 879